Nano Energy 61 (2019) 69–77

Contents lists available at ScienceDirect

Nano Energy

journal homepage: www.elsevier.com/locate/nanoen

Full paper

Crepe cellulose paper and nitrocellulose membrane-based triboelectric nanogenerators for energy harvesting and self-powered human-machine interaction

Sheng Chen[a,b], Jingxian Jiang[b], Feng Xu[a,**], Shaoqin Gong[b,c,*]

[a] Beijing Key Laboratory of Lignocellulosic Chemistry, Beijing Forestry University, Beijing, 100083, China
[b] Wisconsin Institute for Discovery, University of Wisconsin–Madison, Madison, WI, 53706, United States
[c] Department of Biomedical Engineering, Department of Chemistry, and Department of Materials Science and Engineering, University of Wisconsin–Madison, Madison, WI, 53706, United States

ARTICLE INFO

Keywords:
Triboelectric nanogenerator
Crepe cellulose paper
Nitrocellulose membrane
Energy harvesting
Human–machine interaction

ABSTRACT

Cellulose-derived materials have gained a lot of attention for applications in advanced electronics because they are abundant, low cost, lightweight, and sustainable. Herein, we report a paper-based triboelectric nanogenerator (P-TENG) using commercially available materials derived from cellulose by a facile and cost-effective approach. Print paper is used as the substrate, while crepe cellulose paper (CCP) paired with a nitrocellulose membrane (NCM) are used as the friction layers of the P-TENG. CCP and NCM have significantly different tribopolarities and microstructures (i.e., corrugated and porous structures for CPP and NCM, respectively), thereby yielding P-TENGs with outstanding triboelectric performance. For instance, we have demonstrated P-TENGs with an output voltage and current of 196.8 V and 31.5 μA, respectively, a high power density of 16.1 W/m^2, and a robust durability of more than 10,000 cycles. The P-TENGs, as a sustainable power source, can power various electronic devices. Moreover, their great potential applications in self-powered sensing and human–machine interfaces have been demonstrated. Human motion, like a finger touch, can be detected by the P-TENG. A keyboard based on an array of P-TENGs is able to achieve self-powered, real-time communication between a Paper Piano and a computer. This study not only combines the advantages of CCP and NCM to produce high-performance P-TENGs, but also demonstrates the feasibility of using commercially available products to prepare green and sustainable electronics.

1. Introduction

Harvesting mechanical energy from the ambient environment and converting it into electricity have gained increasing attention in recent years because such technologies are crucial to meeting the rising worldwide demand for green and sustainable energy sources [1,2]. As an efficient robust approach to harvesting ubiquitous mechanical energy, triboelectric nanogenerators (TENGs) have been intensely investigated since they first appeared in the literature in 2012 [3]. TENGs are not only low cost and lightweight, they also have a high power output, abundant material choices, and a simple fabrication process, making them attractive devices for harvesting energy [4–6].

TENGs have four basic working modes: vertical contact-separation mode, contact-sliding mode, single-electrode mode, and freestanding triboelectric-layer mode [1,7]. The fundamental theoretical origin of TENGs is Maxwell's displacement current, and the TENGs' operating principle to generate electric energy in an external circuit is coupling the triboelectric effect and electrostatic induction between two materials with different tribopolarities in periodic contact and separation [8,9]. Hence, a TENG is mainly composed of a substrate like polyethylene terephthalate (PET), electrodes (e.g., Cu, Al, and Ag), and two dissimilar materials that work as positive and negative friction layers. Some of the common positive materials utilized to fabricate TENGs include polyamide (PA) and metals (e.g., Cu and Al). The most widely used negative materials in TENGs are polyimide (PI), polyvinylidene fluoride (PVDF), polydimethylsiloxane (PDMS), and polytetrafluoroethylene (PTFE) [8–13]. By combining diverse pairs of these materials, the prepared TENGs have exhibited the capability of harvesting mechanical energy from the ambient environment [4,16] and working as self-powered devices to perform human-motion detection

* Corresponding author. Wisconsin Institute for Discovery, University of Wisconsin–Madison, Madison, WI, 53706, United States.
** Corresponding author.
E-mail addresses: xfx315@bjfu.edu.cn (F. Xu), shaoqingong@wisc.edu (S. Gong).

https://doi.org/10.1016/j.nanoen.2019.04.043
Received 25 February 2019; Received in revised form 9 April 2019; Accepted 10 April 2019
Available online 13 April 2019

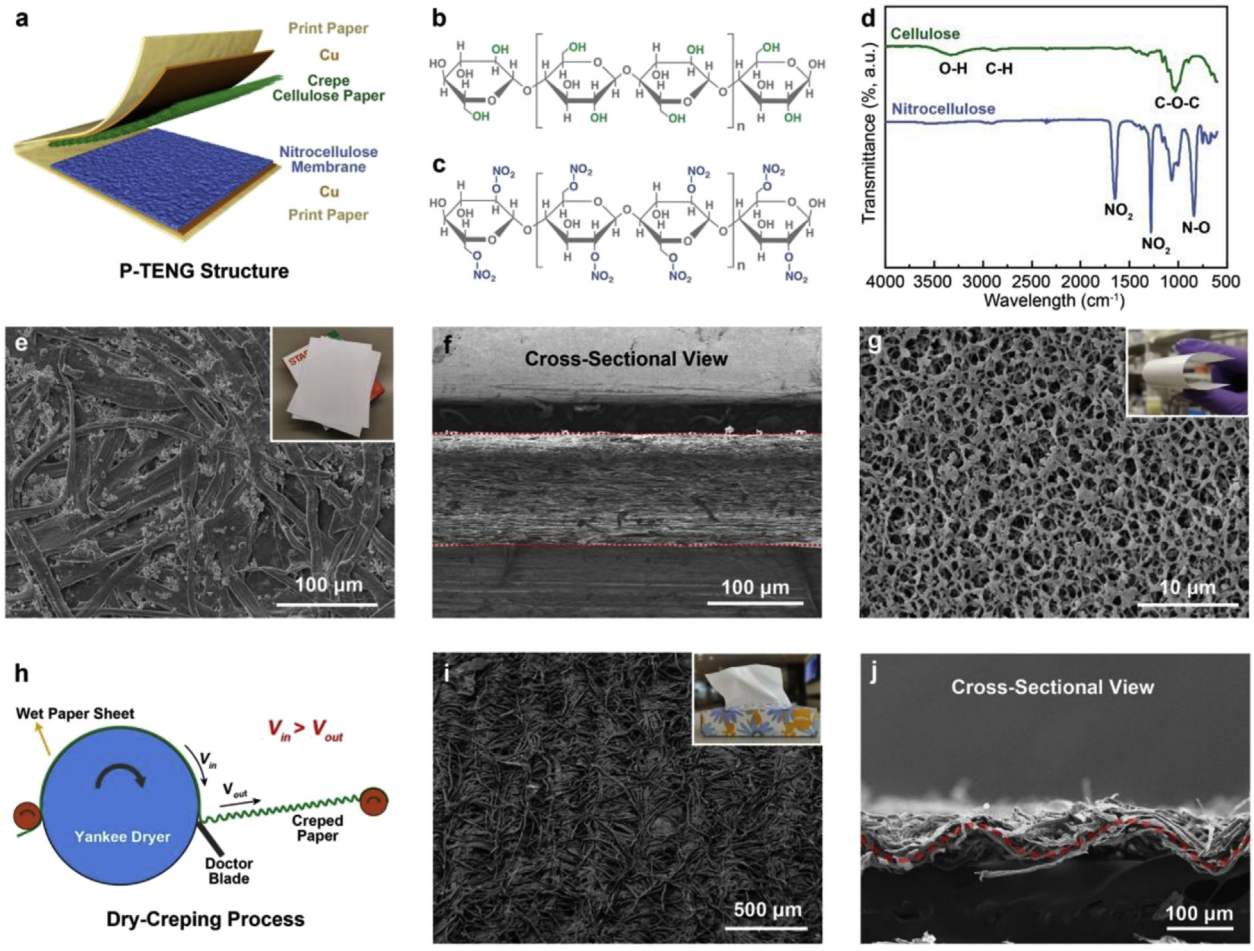

Fig. 1. A triboelectric nanogenerator based on crepe cellulose paper (CCP) and nitrocellulose membrane (NCM) (i.e., P-TENG). (a) Schematic illustration of the P-TENG structure. (b, c) The chemical structure of cellulose and nitrocellulose, respectively. (d) FTIR spectra of the CCP and NCM. (e) An SEM image showing the surface morphology of the print paper as shown in the inset. (f) An SEM image showing the cross-sectional morphology of the print paper. (g) An SEM image showing the porous structure of the flexible NCM as shown in the inset. (h) A schematic illustration of the creping process for CCP in papermaking. (i, j) SEM images showing the corrugated structure of CCP (i: Top view; j: side view). The inset in (i) is a photo of CCP.

[17], pressure sensing [18,19], auditory sensing [20], human–machine interfacing [12,21–23], and wound-healing acceleration [24], to name just a few. However, to date, most materials used in TENGs have been synthetic polymers, which are not renewable, and typically not biodegradable, thereby limiting the further development of cost-effective and environmentally friendly TENGs.

Cellulose and its derivatives are the most abundant natural biomacromolecules. They are widely accessible, renewable, biodegradable, and environmentally benign [25,26]. Cellulose is mainly derived from plants such as wood and cotton. It is commonly used to produce paper (film), textiles, and aerogels [27,28]. Cellulose-based materials have also been used to develop energy-harvesting devices like TENGs in recent years [10,15,29–35]. For example, flexible paper made of cellulose fibers has proven to be a suitable substrate to construct TENGs [15,29]. Additionally, cellulose paper, as well as cellulose nanofibrils films and aerogels, could be used as the positive materials for fabricating effective TENGs [10,30–34].

Although natural cellulose-based materials were used to prepare the TENGs reported previously, some synthetic polymers were still used as friction layers, especially for the negative parts, such as fluorinated ethylene propylene (FEP) [30,33], PVDF [10], PI [32], PTFE [31,35], and PDMS [34]. To address this problem and develop tribonegative materials derived from natural polymers, the nitro group—a strong electron-withdrawing unit—was introduced onto the cellulose film via a chemical reaction to transform the triboelectric polarity of the cellulose from positive to negative [36]. The obtained TENG based on the nitrocellulose film, paired with cellulose or methylcellulose film, demonstrated the potential of utilizing natural, renewable, and biodegradable biomaterials to prepare ecofriendly green TENGs. However, its fabrication process and device structure could be further simplified, and its output performance still has much room for improvement to achieve a wide range of diverse applications.

Besides utilizing suitable material combinations and/or modifying friction materials, increasing the surface area by introducing nano/microstructures in the friction layers is also a promising strategy for improving the output performance of TENGs. The rough surfaces of the friction layers with nano/microstructured patterns and/or arrays significantly enhanced the TENGs' efficiency in harvesting mechanical energy [13,37–40]. Additionally, the porous structure of nanofiber mats and aerogel films could also increase the output performance of prepared TENGs [10,14,34,41]. However, complicated fabrication technologies, such as etching, plasma processing, laser treatment, electrospinning, and freeze-drying, were required in these works. This not only dramatically increased the cost of TENG preparation, but also limited the large-scale development of TENGs for green energy. Therefore, employing cheap, renewable, biodegradable, and commercially available materials to produce high-performance TENGs through simple, cost-effective, and environmentally friendly fabrication processes has become increasingly significant.

In this work, we demonstrated the feasibility of using sustainable

and commercially available crepe cellulose paper (CCP) and nitrocellulose membrane (NCM) to fabricate high-performance, paper-based triboelectric nanogenerators (P-TENGs) through a simple and environmentally friendly approach. Benefiting from the significant difference of tribopolarities between cellulose and nitrocellulose, as well as the differing microstructures (i.e., the corrugated structure in CCP and the porous structure in NCM), the CCP/NCM-based P-TENG exhibited excellent triboelectric performance with an output voltage and current of 196.8 V and 31.5 μA, respectively. It also demonstrated a high power density of 16.1 W/m^2 at a load resistance of 10^6 Ω. The P-TENGs exhibiting good stability and durability can serve as a sustainable power source to drive electronic devices. Moreover, we further demonstrated the potential applications of the P-TENGs in self-powered sensing and human–machine interfacing.

2. Results and discussion

2.1. Fabrication and basic characterization of P-TENGs

The P-TENGs were prepared using commercially available cellulose paper and NCM, both of which are low cost. Fig. 1a is a schematic illustration of the P-TENG structure. It was comprised of folded print paper as the substrate, two electrodes made of conductive copper tape, and two friction layers. The print paper or CCP made of cellulose fibers were used as the tribopositive friction materials; the NCM was used as the tribonegative friction material. The chemical structures of cellulose and nitrocellulose are illustrated in Fig. 1b and c. Cellulose is composed of β-D-glucopyranose units linked by 1,4-glycosidic bonds [42]. The hydroxyl groups on the cellulose were largely replaced by nitro groups in the nitrocellulose. Fig. 1d shows the Fourier transform infrared (FTIR) spectra of the cellulose paper and NCM. The spectrum of cellulose paper presented several peaks around 1028, 2890, and 3325 cm^{-1}, which were associated with the C—O—C pyranose ring skeletal vibration, C—H stretching, and O—H stretching, respectively [43,44]. For the NCM, NO_2 symmetric stretching (1650 and 1279 cm^{-1}) and N—O stretching (839 cm^{-1}) peaks were observed [45]. Moreover, the peak intensity of the O—H stretching in the nitrocellulose dramatically decreased compared with that of cellulose. These findings indicate that abundant nitro groups are present in the NCM.

The morphologies of the cellulose paper and NCM were characterized using a scanning electron microscope (SEM). As shown in Fig. 1e, the print paper made of cellulose fibers had a relatively smooth surface; the flat fibers aggregated and were in close contact with each other. Fig. 1f shows the cross-sectional morphology of the print paper. It had a solid and dense internal structure, which endowed the paper with good stiffness and folding endurance. This allowed the paper to be used as the P-TENG substrate. However, the NCM, composed of randomly oriented nitrocellulose fibers, had a porous structure and a rough surface (Fig. 1g). The porous microstructure exhibited by the NCM, used as the tribonegative friction layer, is expected to enhance the output performance of the P-TENG by inducing a higher triboelectric charge density [46,47].

The morphology and structure of the CCP used as the tribopositive material also play a crucial role in the performance of P-TENGs. For paper products like CCP and the aforementioned print paper, their structures are usually tunable to meet various requirements for different applications via the paper-making process [26,28]. Fig. 1h shows a schematic illustration of the dry-creping process in the production of CCP. After drying on the Yankee dryer, the paper sheet was detached from the cylinder surface using a doctor blade. It should be noted that the speed of the paper sheet moving into the blade was faster than that moving out of the blade, which thereby created many microscopic folds. As can be seen in Fig. 1i and j, the CCP had a rough surface and a corrugated structure. The randomly overlapped cellulose fibers and corrugated structures were designed to increase the surface area of the tribopositive friction layer and thereby improve the output performance of the P-TENGs.

2.2. Triboelectric output performance of P-TENGs

The P-TENGs, with an effective contact area of 6.25 cm^2, were periodically pressed and released (under a force of ~6 N at a frequency of 10 Hz) to study their triboelectric output performance. We first compared the ability of the NCM to gain electrons with other common tribonegative materials by pairing the materials with the print paper as the tribopositive material to assemble the P-TENGs. Figure S1 illustrates the load voltage and short-circuit current (I_{sc}) of these P-TENGs under periodic stress. As significantly negative materials can readily gain electrons, the PI, PVDF, and PTFE endowed the P-TENG devices with good electrical performances; that is, an output voltage higher than 64 V and an output I_{sc} higher than 13.1 μA. The P-TENG with the NCM as the negative friction layer exhibited the highest voltage and I_{sc} values of 103.2 V and 19.4 μA, respectively. This performance was better than that of the PTFE, the most negative material listed in the triboelectric series [1]. Although the nitrocellulose may not have had a greater electron affinity than the PTFE, the better triboelectric performance exhibited by the NCM-based P-TENG may be attributed to the porous structure of the NCM (Fig. 1g). As shown in Figure S2, the solid PTFE film had a smooth surface and dense structure, which might limit triboelectric performance of P-TENG. Therefore, the NCM is a desirable tribonegative material for high-performance P-TENGs.

We further investigated the triboelectric performance of the P-TENGs with the NCM and CCP as tribonegative and tribopositive friction layers, respectively. As shown in Fig. 2a, using CCP significantly improved the device's output voltage from 103.2 V to 144.0 V as compared to using print paper. The I_{sc} also showed the same trend of increased electrical signals (from 19.4 μA to 24.6 μA) for the CCP-based P-TENG, as demonstrated in Fig. 2b. This output enhancement may be attributable to the rough surface and corrugated structure of the CCP (Fig. 1i and j), which would significantly increase the P-TENG's effective contact area and, therefore, its triboelectric charge density [47,48].

The P-TENGs fabricated with a different number of CCP layers had different thicknesses and internal structures, which would affect the output performance of the devices. Fig. 2c and d shows the output voltage of the P-TENGs with various layers of CCP paired with a single layer of the NCM. The voltage increased from 144.0 V to 196.8 V when the number of CCP layers increased from one to three. However, the voltage decreased to 136.0 V when the number of CCP layers further increased to six. The output current also had a similar change trend: the P-TENG with 3 layers of CCP exhibited the highest output I_{sc} of 31.5 μA when compared to other devices, as demonstrated in Fig. 2e and f. To further study the effect of the number of CCP layers on the electrical performance of P-TENGs, we measured the thickness of the multi-layer CCP and the results are shown in Figure S3. One layer of CCP had a thickness of only ~51 μm. When the number of layers increased to six, the thickness of the multi-layer CCP increased to ~249 μm. However, the increase in thickness was nonlinear; the total value was less than the single layer thickness multiplied by the number of CCP layers. This may be attributable to the CCP's softness, which endowed it with compressibility, and the interdigitated corrugated structure between the layers of CCPs, as shown by the inset illustrations in Figure S3. The overlapping multi-layer CCP created a porous internal structure. As previously reported, porous friction layers in a TENG device with a proper thickness would improve the output performance due to the increased charges in contact, which was generated on both the outermost surface and inner porous surface of the friction layer [10,11,34]. However, thickened friction layers would increase the distance between the friction surface and the induction electrodes; hence, a greater induction distance would yield fewer induced charges due to the edge effect of electrostatic induction [49]. Therefore, the over-thick friction layers may reduce the device's output performance [11,50]. Additionally, when the paper substrate had a constant folding angle in the releasing

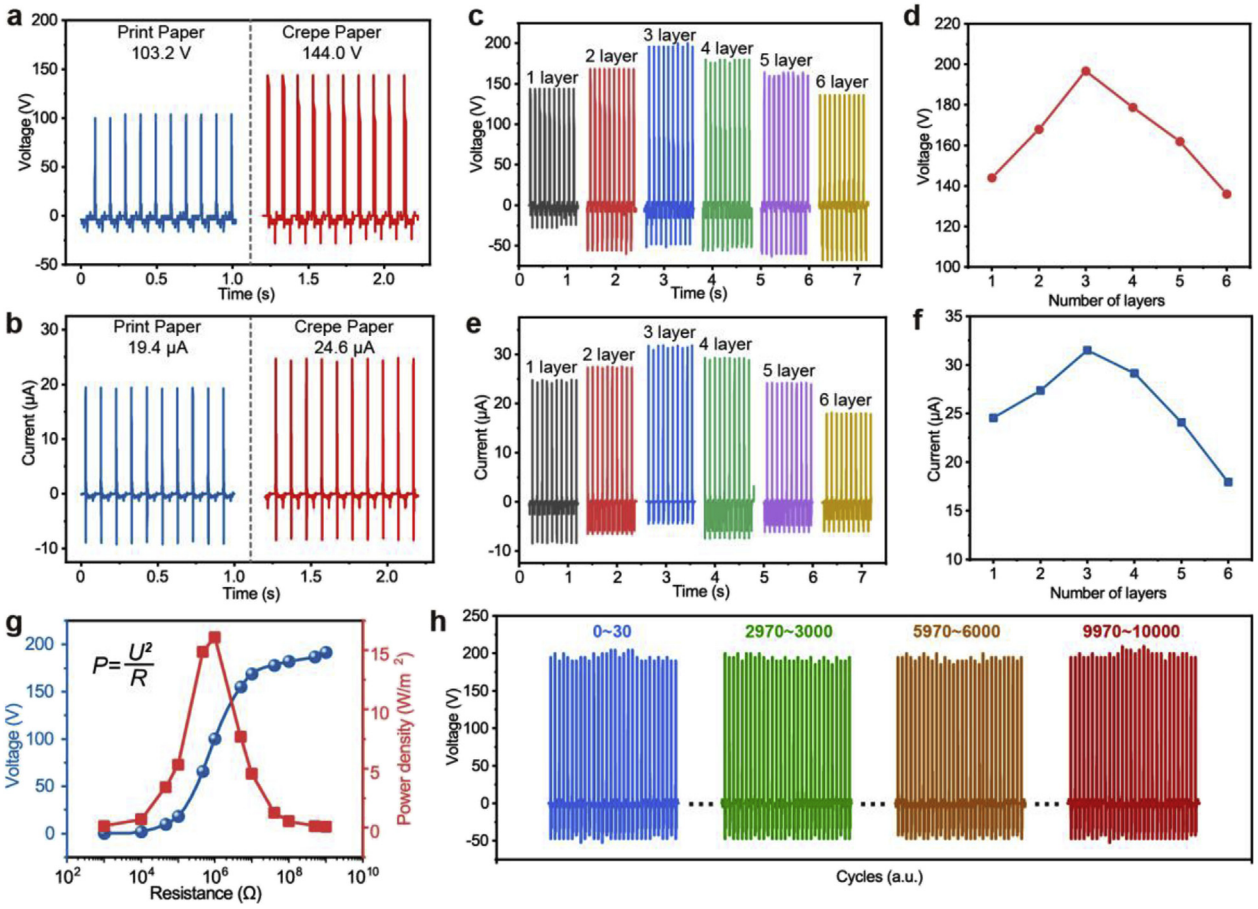

Fig. 2. Triboelectric performance of the P-TENGs under periodic stress at a frequency of 10 Hz. (a) Load voltage output and (b) short-circuit current output (I_{sc}) of P-TENGs comprised of print paper or CCP as the positive friction layer and NCM as the negative friction layer. (c) Load voltage output and (e) short-circuit current output of P-TENGs comprised of an NCM as the negative friction layer and varying multi-layer (1–6 layers) of CCP as the positive friction layer. (d, f) Average peak voltage and current of P-TENGs comprised of an NCM as the negative friction layer and multi-layer of CCP as the positive friction layer. (g) Output voltage and power density of a P-TENG comprised of 3-layer CCP and an NCM as friction layers on external load resistance. (h) Output voltage of a P-TENG comprised of 3-layer CCP and an NCM as friction layers for 10,000 press and release cycles, demonstrating good stability and durability of the P-TENG.

state during the press/release cycle, the increased number of CCP layers (i.e., friction layer thickness) would cause a decreased air gap distance and thereby limit the potential electrical output for P-TENGs [11,51]. Therefore, the number of CCP layers simultaneously had a positive and negative effect on the electrical performance of the P-TENGs, and thus there was an optimum number of layers—i.e., three—for the CCP/NCM-based P-TENG.

The output power density and stability of the P-TENG with three layers of CCP were further investigated due to this device's superior triboelectric output performance. The dependence of the output voltage on the load resistance was measured by connecting various resistors, ranging from 10^3 to $10^9\,\Omega$, to the P-TENG. As shown in Fig. 2g, the output voltage of the P-TENG increased with an increase in the external loading. The output power is determined by the following equation [41],

$$P = \frac{U^2}{R}$$

where U and R stand for the output voltage of the P-TENG and the loading resistance, respectively. The output power density first increased, and then decreased, as the load resistance increased. According to the maximum power transfer theorem, the maximum output power can be obtained when the external load resistance equals the internal impedance of the P-TENG [52,53]. Therefore, a maximum peak power density of 16.1 W/m^2 was achieved at a load resistance of $10^6\,\Omega$. This high amount of power delivered was sufficient to drive some portable and/or wearable electronics and charge energy storage devices, thus expanding the application range of P-TENGs.

The durability and stability of the P-TENGs are also crucial and important to their practical utilization. As shown in Fig. 2h, no obvious difference in output voltage was observed during the 10,000 press–-release cycles. The triboelectric outputs were recorded after the P-TENG was operating for several minutes to allow the P-TENG to reach steady state. Generally, the P-TENG exhibited an increased peak output voltage during the initial stage before reaching steady state (Figure S4). Furthermore, the output voltage was well maintained for the P-TENG after storage in ambient air (~40% relative humidity (RH)) for 75 days (Figure S5). These results, which show a stable output performance, demonstrate the excellent durability and reliability of the P-TENG. In addition, the humidity of the operating environment is a critical factor affecting the triboelectric performance of TENGs. Its effect on the output voltage of the P-TENG was investigated and is shown in Figure S6. The peak output voltage of the P-TENG decreased from around 195 to 9 V as the RH increased from 40% to 85%, which may be attributed to the weakened triboelectric effect under high RH [54,55]. This indicates that the P-TENG we prepared has limited utility in harsh environments with high RHs. However, its great sensitivity to RH may endow the P-TENG with the potential to be used for humidity detection [56].

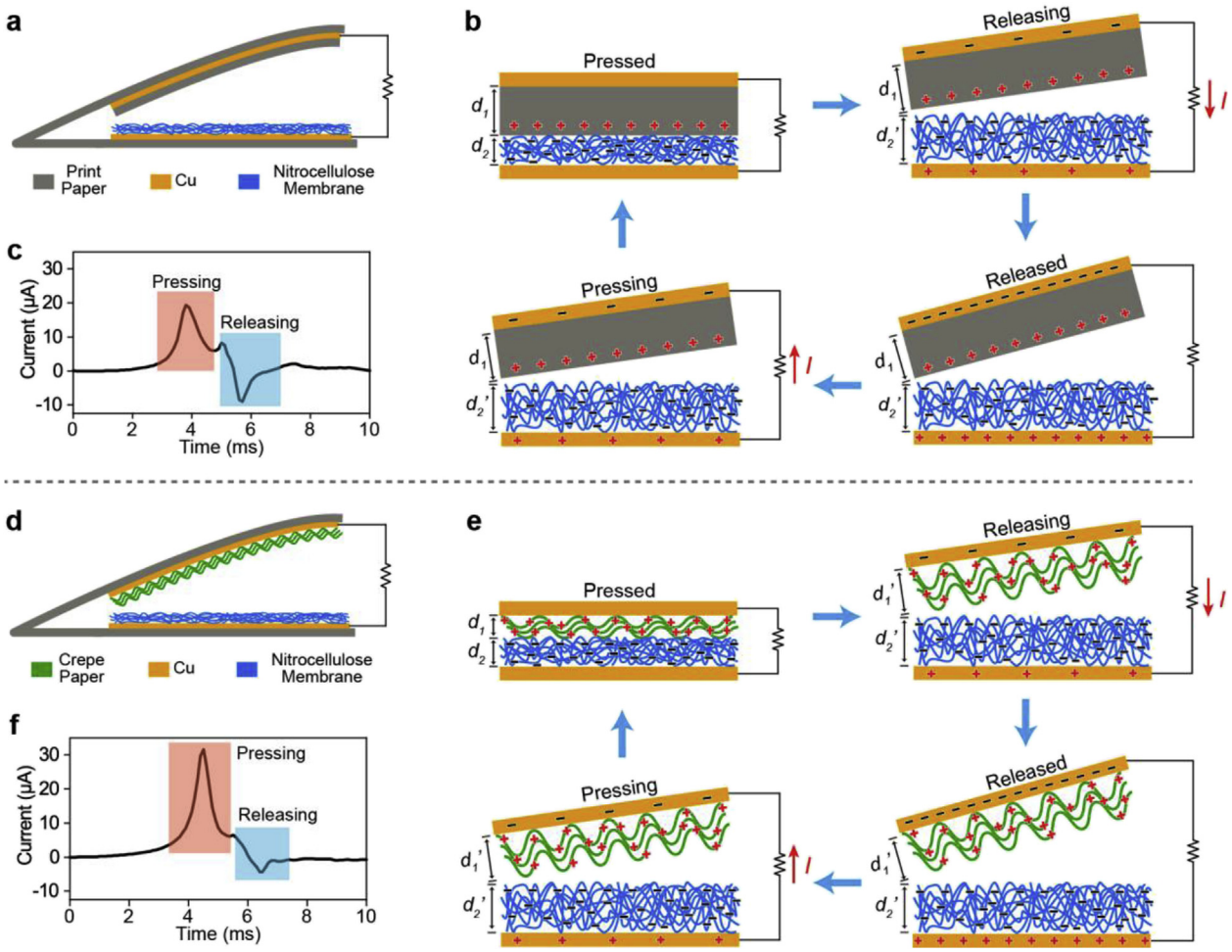

Fig. 3. Schematic illustration of the P-TENG working principle. (a, b) Working principle of the P-TENG containing print paper as the positive friction layer, and its (c) short-circuit current output under one cycle of pressing and releasing. (d, e) Working principle of the P-TENG containing three layers of CCP as the positive friction layer and its (f) short-circuit current output under one cycle of pressing and releasing.

2.3. Working principle of P-TENGs

The working mechanism of the P-TENG is based on the coupling effect of contact electrification and electrostatic induction [57,58], which is demonstrated by the schematic illustration in Fig. 3. For the P-TENG with print paper as both the substrate and the tribopositive friction layer, no charges were generated on the friction layers in the original state (Fig. 3a). Under external force, the P-TENG generated electrical output during cyclic pressing and releasing (Fig. 3b). When in contact with each other, the print paper tended to lose electrons while the NCM tended to gain electrons. Therefore, positive charges were generated on the surface of the dense print paper, while negative charges were generated on both the surface and the interior pores of the porous NCM. As the external force was withdrawn, the P-TENG started to release under the restoring force from the substrate (print paper). The separated friction layers caused an electric potential difference between the two electrodes, thus driving the electrons flowing from the bottom electrode to the top electrode through external loads. When the friction layers were released completely, the triboelectric charges were totally neutralized and no electrical signals were generated. Meanwhile, when the print paper and the NCM were getting close to each other during the pressing cycle, the potential in the bottom electrode became higher and caused the electrons to flow back from the top electrode to the bottom electrode through the external circuit. The flow direction of the electrons was opposite that of the current direction. The related electric current generated from the P-TENG under external periodic forces is shown in Fig. 3 (c). The pressing and releasing cycles generated current signals with opposite directions. It was also found that the output current peak corresponding to pressing was higher than that for releasing. This may be attributed to the smaller restoring force from the paper substrate, and thus a slower separation of friction layers for releasing, compared with the faster pressing process under a larger external force [59–61].

The P-TENG with multi-layer CCP as the tribopositive friction layers had a similar operating principle (Fig. 3d). However, compared with the smooth and dense print paper in the aforementioned case, the multi-layer CCP induced a larger amount of positive charges on both the contact surface and the surface of the interior pores due to their higher surface area and compressed porous structures (Fig. 3e). This led to a larger electrical potential difference between the top and bottom electrodes, thus yielding a higher output current for the P-TENG under cyclic pressing, as demonstrated in Fig. 3f.

Supplementary data related to this article can be found at https://doi.org/10.1016/j.nanoen.2019.04.043.

2.4. Applications of P-TENGs for energy harvesting and self-powered sensing

Supplementary data related to this article can be found at https://doi.org/10.1016/j.nanoen.2019.04.043.

To study the practical applications of the P-TENG for harvesting mechanical energy and performing self-powered sensing, several small

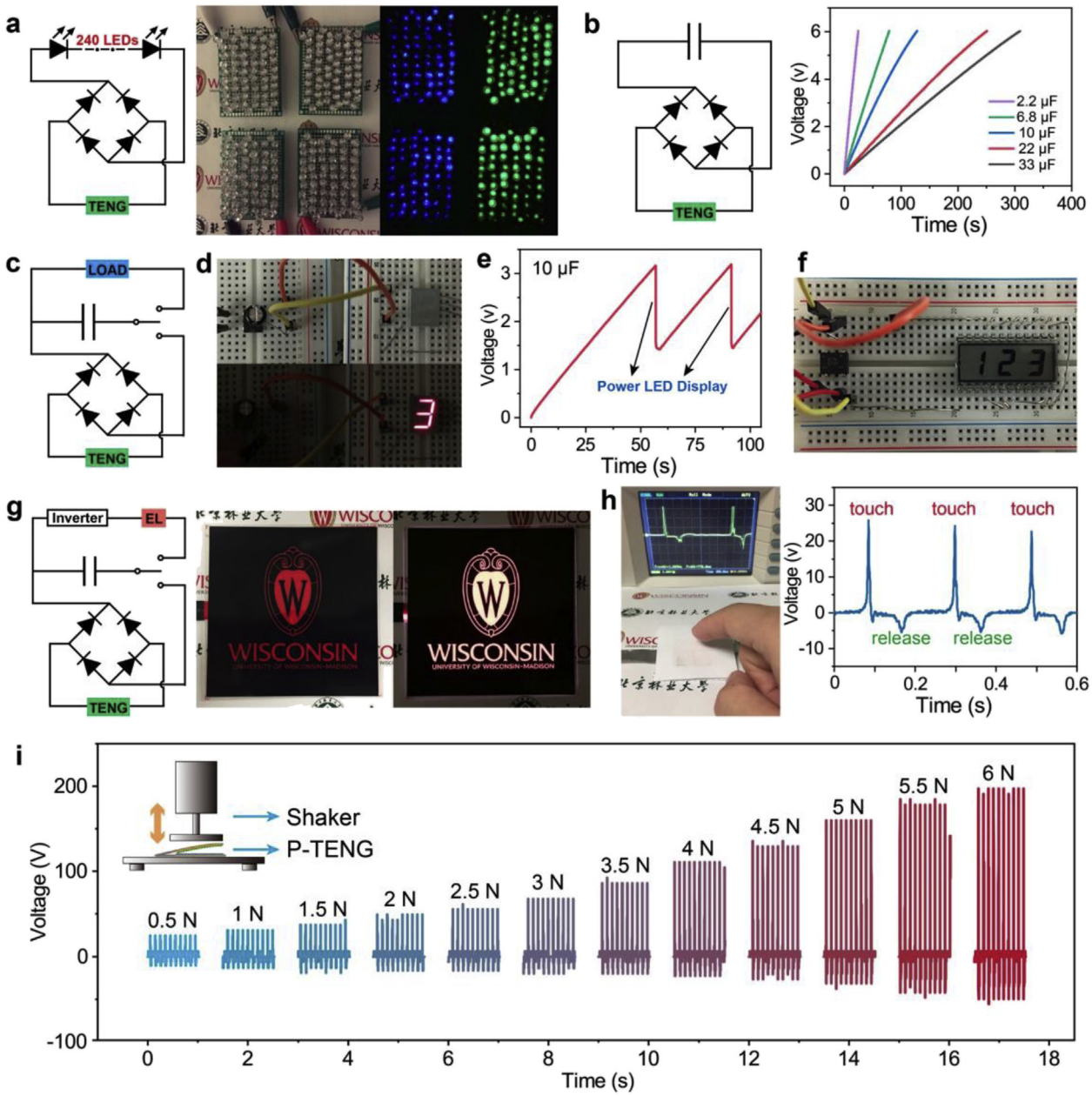

Fig. 4. Energy harvesting and self-powered touch sensing by the P-TENG made of three layers of CCP and a NCM as the friction layers with an effective size of 6.25 cm^2. (a) The P-TENG could light up 240 LEDs through a bridge rectifier under repeated pressing (9.6 kPa) at a frequency of 10 Hz. (b) The P-TENG could charge capacitors with different capacitances up to 6 V with a bridge rectifier. (c, d, e, f) A segmented LED display and an LCD were powered by a 10 μF capacitor charged by the P-TENG. (g) An electroluminescence (EL) display containing the University of Wisconsin–Madison logo was powered using a P-TENG charged capacitor (10 μF). (h) Demonstration of self-powered touch sensing using the P-TENG. (i) Output voltage of the P-TENG under periodic pressing by a shaker with different applied forces.

electronic devices were driven and finger touch was measured using the optimum P-TENG, which consisted of three layers of CCP as the tribo-positive friction material (Fig. 4). The P-TENG, under periodic stress, was able to light up 240 light-emitting-diodes (LEDs) connected in series through a commercial bridge rectifier (Fig. 4a and Video S1). This demonstrates the excellent ability of the P-TENG to convert mechanical energy to electrical output. However, the generated electrical energy from the P-TENG was alternating, which is not applicable for directly driving most electronics. Therefore, energy storage devices, such as batteries or capacitors, are used to store the harvested energy from the P-TENG first. For demonstration, the P-TENG was used to charge different types of capacitors through a bridge rectifier under an external force of ~6 N at a frequency of 10 Hz (Fig. 4b). The 2.2 μF capacitor was rapidly charged to 6 V within only 24 s by the P-TENG. The 22 μF and 33 μF capacitors were charged to 6 V in 249 and 307 s, respectively. This demonstrates that the P-TENG is an efficient energy harvesting power source. The charged capacitor (10 μF) was further used to power several small electronic devices, such as a segmented LED display, a liquid crystal display (LCD), and an electroluminescence (EL) display unit. Fig. 4c shows a schematic circuit diagram using the P-TENG to charge a capacitor, which was further used to drive electronic devices. The LED segment display showing "3" was turned on by the charged capacitor (Fig. 4d). However, the energy stored in the capacitor was rapidly consumed; therefore, repetitive charging of capacitors by the P-TENG was required for practical utilization, as demonstrated by the changed voltage of the charged capacitor before and after powering the

LED segment display in Fig. 4e. Additionally, an LCD showing "1 2 3" with low power consumption could be powered using the charged capacitor for a longer period of time (Fig. 4f). An EL display unit showing the University of Wisconsin–Madison logo was also activated by the capacitor, which was charged by the P-TENG connected with an inverter (Fig. 4g).

The P-TENG can also sense external force, because it is able to generate electrical signals in response to forces applied to it. Moreover, an external power source is not required to provide energy to the P-TENG, compared to conventional strain/pressure sensors that are based on the capacitive [62] or piezoresistive [63] principle. By contrast, the P-TENG sensor is able to achieve self-powered sensing. As shown in Fig. 4h and Video S2, the pressure changes caused by a finger touch and release are detected in real-time by the P-TENG. The output voltage of the P-TENG under periodic pressing with different forces was investigated and is shown in Fig. 4i. As can be seen, the output peak voltage increases with the increased applied force. The linear relationship between the output peak voltage and the applied force was further demonstrated in Figure S7. The P-TENG exhibited a high sensitivity of 31.85 $V N^{-1}$ in the range of 0.5–6 N. These results indicate that the P-TENG has the potential to be used in the detection of external forces such as human motion.

2.5. P-TENG-based paper piano for self-powered human–machine interfacing

Supplementary data related to this article can be found at https://doi.org/10.1016/j.nanoen.2019.04.043.

Employing a simple fabrication process, as well as cuttable and foldable materials, a paper piano using an array of P-TENGs as the keyboard was designed and fabricated for self-powered human–machine interactions. As shown by the photograph in Fig. 5a, the keyboard for the paper piano was made of a 1 × 7 array of P-TENGs. The structure of each key (i.e., P-TENG), as highlighted by the red dashed-line rectangle, is illustrated by the schemes in Fig. 5b. Folded print paper was used as the substrate for the whole device. The flat print paper and NCM were used as the tribopositive and tribonegative friction parts of the P-TENG, respectively. The Cu foil was used as the electrodes and further connected to the computer for human–machine interfacing. As shown by the circuit diagram in Fig. 5c, the P-TENG-based keyboard with bridge rectifiers and capacitors was connected to a laptop with a speaker through a microcontroller (the detailed pin connections are shown in Figure S8). When pressing and releasing the keys of the P-TENG-based keyboard, the related capacitors were charged. As an example, the voltage of the capacitor connected to the "DO" key under cyclic pressing was measured and is shown in Figure S9. Every finger press caused a step voltage increase of the capacitor. These voltage changes in the capacitors were measured and recorded using a microcontroller, which made it possible for real-time communication between the keyboard and a computer via a homemade MATLAB program (the MATLAB code used is shown in the Supporting Information).

Fig. 5d and Video S3 demonstrate the self-powered human–machine interface using the paper piano-based array of P-TENGs. The part of the song named *Twinkle Twinkle Little Star* was played using the paper piano by pressing the related keys. The pressed key (i.e., P-TENG) generated electrical energy used to charge the capacitors. The voltage changes were further used to control the sound program as input signals. Since the signal generation in this case did not need an external power source, the self-powered human–machine interaction was achieved by the P-TENGs.

3. Conclusions

A cellulose-derived material-based TENG was designed and fabricated via a facile fabrication approach. Taking advantage of both the significantly different tribopolarities between the CCP and NCM, and their microstructures (i.e., corrugated and porous structures, respectively), the CCP/NCM-based P-TENGs exhibited excellent triboelectric performances, including a high power density of 16.1 W/m^2 and a good durability of over 10,000 cycles. The P-TENGs further demonstrated the capability of harvesting mechanical energy, as well as self-powered sensing and human–machine interfacing. Furthermore, the P-TENGs we reported here have the following advantages: both the substrate (i.e., print paper) and the friction materials (i.e., the CCP and NCM) were (1) derived from earth-abundant, renewable, and biodegradable cellulose; (2) commercially available and scalable at a low cost; (3) comprised of microstructures that enhance the triboelectric performance of the P-TENGs; and (4) can be assembled through a simple, cost-effective, and environmentally friendly process to produce the P-TENG devices. Additionally, this work demonstrates the feasibility of using commercially available products to prepare green and sustainable electronics.

4. Experimental section

4.1. Fabrication of P-TENGs

A piece of commercial print paper (75 g/m^2, Staplex) was trimmed to a custom size (11 × 5 cm^2) and used as the substrate of the P-TENGs. Commercially available crepe cellulose paper (CCP, Kleenex tissue) and nitrocellulose membrane (NCM, pore size: 0.2 μm, WestClear) with a size of 2.5 × 2.5 cm^2 were used as the positive friction layer and negative friction layer, respectively. Copper (Cu) foils were used as the electrodes. The friction layers and electrodes were attached onto the opposite sides of the paper substrate. The whole device was then folded to make the friction layers face each other. For comparison, the TENGs with other tribopositive and/or tribonegative layers were fabricated following the same procedure.

4.2. Characterization and triboelectric measurements

The surface and cross-sectional morphologies of the print paper, CCP, and NCM were characterized via SEM (Jeol Neoscope JCM-5000). FTIR spectra were obtained using a Tensor 27 spectrometer (Bruker, USA) with a resolution of 4 cm^{-1}. The thickness of the multi-layer CCP was measured by a digital micrometer (Shars). The output performance of the P-TENGs was characterized by applying a vertical force. The P-TENGs were periodically pressed using a shaker (LDS V201, Bruel & Kjer, Denmark), which was controlled by a function generator (B&K Precision) and a power amplifier (Yamaha). The voltage and current output signals were measured using an oscilloscope (DS1102E, Rigol, China) with an input impedance of 100 MΩ and a potentiostat (VersaSTAT-3, Princeton Applied Research, USA), respectively.

4.3. Paper piano for self-powered human–machine interfacing

The self-powered paper piano was made of a 1 × 7 array of P-TENGs that were connected to a computer. Commercial print paper (75 g/m^2, Staplex) was used as both the substrate and the tribopositive friction layer of the P-TENG-based keyboard. The NCM and Cu foil were used as the negative friction layer and the electrodes, respectively. To perform human–machine interfacing and communication using the self-powered paper piano, the P-TENGs in the keyboard were used to charge capacitors (0.22 μF) through bridge rectifiers; the voltage changes in these capacitors were measured and recorded by a microcontroller (Arduino Mega 2560), which was connected to a computer using a homemade MATLAB (MathWorks, USA) program.

Acknowledgements

The authors gratefully acknowledge the financial support from the University of Wisconsin-Madison and the China Scholarship Council.

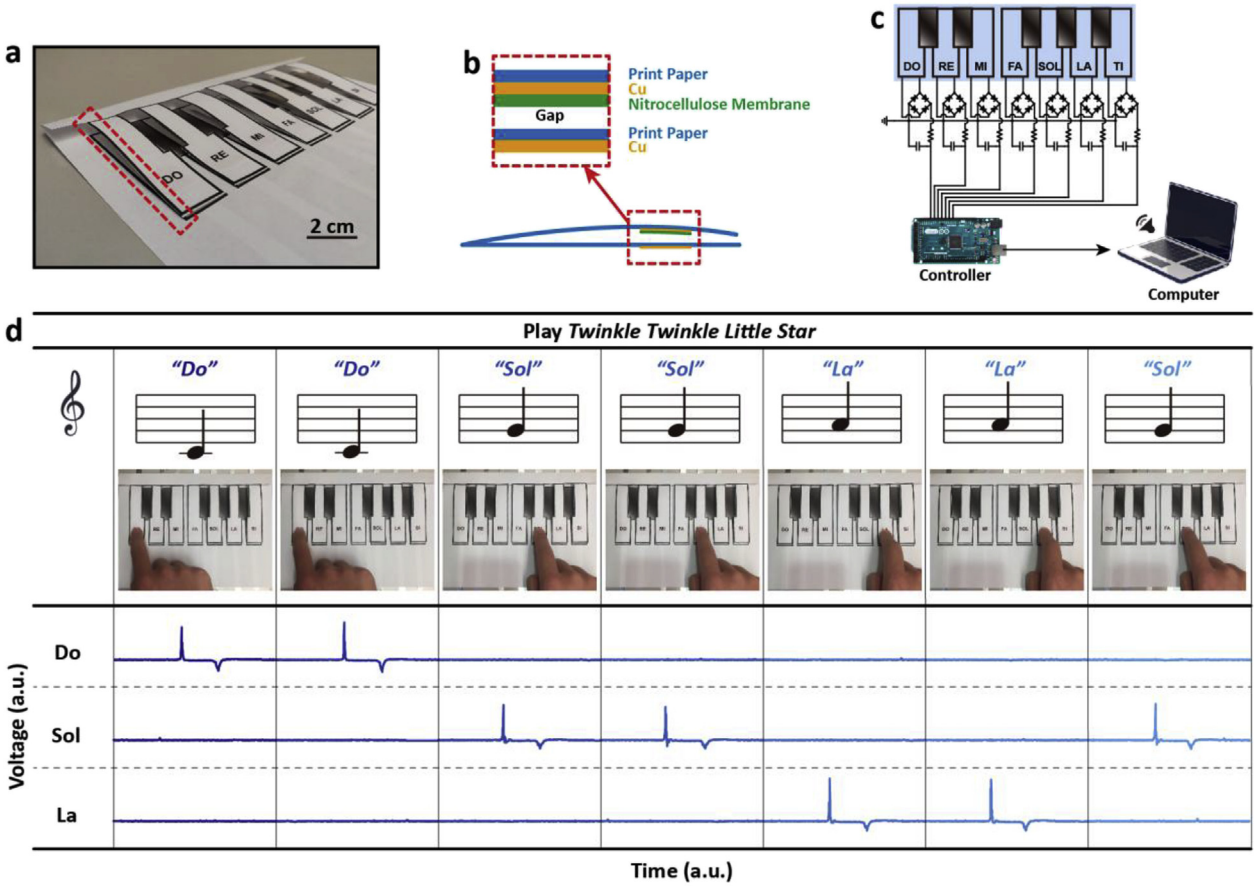

Fig. 5. P-TENG-based paper piano for self-powered human–machine interfacing. (a) Photo of the self-powered paper piano consisting of a 1 × 7 P-TENG array. (b) Schematic illustration of the structure of each key; i.e., the P-TENG. (c) Circuit diagram of the paper piano connected with a computer through a microcontroller. (d) Demonstration of the self-powered paper piano playing a song.

Appendix A. Supplementary data

Supplementary data related to this article can be found at https://doi.org/10.1016/j.nanoen.2019.04.043.

References

[1] Z.L. Wang, ACS Nano 7 (2013) 9533–9557.
[2] C.S. Wu, A.C. Wang, W.B. Ding, H.Y. Guo, Z.L. Wang, Adv. Energy Mater. 9 (2019) 25.
[3] F.-R. Fan, Z.-Q. Tian, Z.L. Wang, Nano Energy 1 (2012) 328–334.
[4] P. Bai, G. Zhu, Z.-H. Lin, Q. Jing, J. Chen, G. Zhang, J. Ma, Z.L. Wang, ACS Nano 7 (2013) 3713–3719.
[5] G. Zhu, Z.-H. Lin, Q. Jing, P. Bai, C. Pan, Y. Yang, Y. Zhou, Z.L. Wang, Nano Lett. 13 (2013) 847–853.
[6] X. Chen, K. Parida, J. Wang, J. Xiong, M.-F. Lin, J. Shao, P.S. Lee, ACS Appl. Mater. Interfaces 9 (2017) 42200–42209.
[7] Z.L. Wang, Faraday Discuss 176 (2014) 447–458.
[8] Z.L. Wang, Mater. Today 20 (2017) 74–82.
[9] J. Shao, M. Willatzen, T. Jiang, W. Tang, X. Chen, J. Wang, Z.L. Wang, Nano Energy 59 (2019) 380–389.
[10] H.Y. Mi, X. Jing, Q.F. Zheng, L.M. Fang, H.X. Huang, L.S. Turng, S.Q. Gong, Nano Energy 48 (2018) 327–336.
[11] H.Y. Mi, X. Jing, M.A.B. Meador, H.Q. Guo, L.S. Turng, S.Q. Gong, ACS Appl. Mater. Interfaces 10 (2018) 30596–30606.
[12] X. He, Y.L. Zi, H. Yu, S.L. Zhang, J. Wang, W.B. Ding, H.Y. Zou, W. Zhang, C.H. Lu, Z.L. Wang, Nano Energy 39 (2017) 328–336.
[13] Y. Song, X.L. Cheng, H.T. Chen, J.H. Huang, X.X. Chen, M.D. Han, Z.M. Su, B. Meng, Z.J. Song, H.X. Zhang, J. Mater. Chem. 4 (2016) 14298–14306.
[14] B. Yu, H. Yu, T. Huang, H. Wang, M. Zhu, Nano Energy 48 (2018) 464–470.
[15] Q.Z. Zhong, J.W. Zhong, B. Hu, Q.Y. Hu, J. Zhou, Z.L. Wang, Energy Environ. Sci. 6 (2013) 1779–1784.
[16] Y. Yang, G. Zhu, H.L. Zhang, J. Chen, X.D. Zhong, Z.H. Lin, Y.J. Su, P. Bai, X.N. Wen, Z.L. Wang, ACS Nano 7 (2013) 9461–9468.
[17] G.H. Lim, S.S. Kwak, N. Kwon, T. Kim, H. Kim, S.M. Kim, S.W. Kim, B. Lim, Nano Energy 42 (2017) 300–306.
[18] M.Y. Ma, Z. Zhang, Q.L. Liao, F. Yi, L.H. Han, G.J. Zhang, S. Liu, X.Q. Liao, Y. Zhang, Nano Energy 32 (2017) 389–396.
[19] K.Y. Lee, H.J. Yoon, T. Jiang, X.N. Wen, W. Seung, S.W. Kim, Z.L. Wang, Adv. Energy Mater. 6 (2016).
[20] H. Guo, X. Pu, J. Chen, Y. Meng, M.-H. Yeh, G. Liu, Q. Tang, B. Chen, D. Liu, S. Qi, Science Robotics 3 (2018) eaat2516.
[21] R. Cao, X.J. Pu, X.Y. Du, W. Yang, J.N. Wang, H.Y. Guo, S.Y. Zhao, Z.Q. Yuan, C. Zhang, C.J. Li, Z.L. Wang, ACS Nano 12 (2018) 5190–5196.
[22] X. Pu, H. Guo, J. Chen, X. Wang, Y. Xi, C. Hu, Z.L. Wang, Sci. Adv. 3 (2017) e1700694.
[23] X. Pu, H. Guo, Q. Tang, J. Chen, L. Feng, G. Liu, X. Wang, Y. Xi, C. Hu, Z.L. Wang, Nano Energy 54 (2018) 453–460.
[24] Y. Long, H. Wei, J. Li, G. Yao, B. Yu, D. Ni, A.L. Gibson, X. Lan, Y. Jiang, W. Cai, ACS Nano 12 (2018) 12533–12540.
[25] C. Wu, T.W. Kima, S. Sung, J.H. Park, F. Li, Nano Energy 44 (2018) 279–287.
[26] S. Chen, Y. Song, D. Ding, Z. Ling, F. Xu, Adv. Funct. Mater. 28 (2018) 1802547.
[27] H. Jin, Y. Nishiyama, M. Wada, S. Kuga, Colloid. Surf. Physicochem. Eng. Asp. 240 (2004) 63–67.
[28] S. Chen, Y. Song, F. Xu, ACS Sustain. Chem. Eng. 6 (2018) 5173–5181.
[29] H.Y. Guo, M.H. Yeh, Y.L. Zi, Z. Wen, J. Chen, G.L. Lin, C.G. Hu, Z.L. Wang, ACS Nano 11 (2017) 4475–4482.
[30] X. He, H. Zou, Z. Geng, X. Wang, W. Ding, F. Hu, Y. Zi, C. Xu, S.L. Zhang, H. Yu, Adv. Funct. Mater. 28 (2018) 1805540.
[31] Y.C. Mao, N. Zhang, Y.J. Tang, M. Wang, M.J. Chao, E.J. Liang, Nanoscale 9 (2017) 14499–14505.
[32] C. Wu, J.H. Park, S. Sung, B. Koo, Y.H. Lee, T.W. Kim, Nano Energy 51 (2018) 383–390.
[33] C.H. Yao, A. Hernandez, Y.H. Yu, Z.Y. Cai, X.D. Wang, Nano Energy 30 (2016) 103–108.
[34] Q. Zheng, L. Fang, H. Guo, K. Yang, Z. Cai, M.A.B. Meador, S. Gong, Adv. Funct. Mater. 28 (2018) 1706365.
[35] K.Q. Xia, H.Z. Zhang, Z.Y. Zhu, Z.W. Xu, Sensor Actuator Phys. 272 (2018) 28–32.
[36] C. Yao, X. Yin, Y. Yu, Z. Cai, X. Wang, Adv. Funct. Mater. 27 (2017) 1700794.
[37] Z. Lin, J. Chen, X. Li, Z. Zhou, K. Meng, W. Wei, J. Yang, Z.L. Wang, ACS Nano 11 (2017) 8830–8837.
[38] H.S. Wang, C.K. Jeong, M.H. Seo, D.J. Joe, J.H. Han, J.B. Yoon, K.J. Lee, Nano Energy 35 (2017) 415–423.
[39] R.X. Wang, S.J. Gao, Z. Yang, Y.L. Li, W.N. Chen, B.X. Wu, W. Wu, Adv. Mater. 30

(2018) 201706267.
[40] W. Yang, J. Chen, Q. Jing, J. Yang, X. Wen, Y. Su, G. Zhu, P. Bai, Z.L. Wang, Adv. Funct. Mater. 24 (2014) 4090–4096.
[41] B. Yu, H. Yu, H. Wang, Q. Zhang, M. Zhu, Nano Energy 34 (2017) 69–75.
[42] A.C. O'sullivan, Cellulose 4 (1997) 173–207.
[43] H. Yang, R. Yan, H. Chen, D.H. Lee, C. Zheng, Fuel 86 (2007) 1781–1788.
[44] T. Kondo, C. Sawatari, Polymer 37 (1996) 393–399.
[45] V. Kovalenko, R. Mukhamadeeva, L. Maklakova, N. Gustova, J. Struct. Chem. 34 (1994) 540–547.
[46] Y. Yang, H. Zhang, Z.-H. Lin, Y.S. Zhou, Q. Jing, Y. Su, J. Yang, J. Chen, C. Hu, Z.L. Wang, ACS Nano 7 (2013) 9213–9222.
[47] Y. Jie, H.R. Zhu, X. Cao, Y. Zhang, N. Wang, L.Q. Zhang, Z.L. Wang, ACS Nano 10 (2016) 10366–10372.
[48] M.-L. Seol, J.-H. Woo, S.-B. Jeon, D. Kim, S.-J. Park, J. Hur, Y.-K. Choi, Nano Energy 14 (2015) 201–208.
[49] Y. Lu, X. Wang, X. Wu, J. Qin, R. Lu, J. Micromech. Microeng. 24 (2014) 065010.
[50] G. Zhu, Y.S. Zhou, P. Bai, X.S. Meng, Q.S. Jing, J. Chen, Z.L. Wang, Adv. Mater. 26 (2014) 3788–3796.
[51] S. Niu, Z.L. Wang, Nano Energy 14 (2015) 161–192.
[52] F. Xing, Y. Jie, X. Cao, T. Li, N. Wang, Nano Energy 42 (2017) 138–142.
[53] X. Yang, S. Chan, L. Wang, W.A. Daoud, Nano Energy 44 (2018) 388–398.
[54] K.Y. Lee, J. Chun, J.H. Lee, K.N. Kim, N.R. Kang, J.Y. Kim, M.H. Kim, K.S. Shin, M.K. Gupta, J.M. Baik, Adv. Mater. 26 (2014) 5037–5042.
[55] Z. Zhang, Z. Bai, Y. Chen, J. Guo, Nano Energy 58 (2019) 759–767.
[56] H. Guo, J. Chen, L. Tian, Q. Leng, Y. Xi, C. Hu, ACS Appl. Mater. Interfaces 6 (2014) 17184–17189.
[57] L. Zheng, Z.-H. Lin, G. Cheng, W. Wu, X. Wen, S. Lee, Z.L. Wang, Nano Energy 9 (2014) 291–300.
[58] B. Meng, W. Tang, Z.-h. Too, X. Zhang, M. Han, W. Liu, H. Zhang, Energy Environ. Sci. 6 (2013) 3235–3240.
[59] J. Chen, G. Zhu, W. Yang, Q. Jing, P. Bai, Y. Yang, T.C. Hou, Z.L. Wang, Adv. Mater. 25 (2013) 6094–6099.
[60] M. Ma, Q. Liao, G. Zhang, Z. Zhang, Q. Liang, Y. Zhang, Adv. Funct. Mater. 25 (2015) 6489–6494.
[61] G. Zhu, C. Pan, W. Guo, C.-Y. Chen, Y. Zhou, R. Yu, Z.L. Wang, Nano Lett. 12 (2012) 4960–4965.
[62] S. Wan, H. Bi, Y. Zhou, X. Xie, S. Su, K. Yin, L. Sun, Carbon 114 (2017) 209–216.
[63] S. Chen, Y. Song, F. Xu, ACS Appl. Mater. Interfaces 10 (2018) 34646–34654.

Sheng Chen received a Bachelor's degree in Chemical Processing Engineering of Forest Products from Beijing Forestry University in 2015. He is currently a PhD candidate in Chemical Processing Engineering of Forest Products at the College of Materials Science and Technology, Beijing Forestry University. At present, he is a visiting PhD student at the Wisconsin Institute for Discovery, University of Wisconsin–Madison. His current research focuses on biomass-derived functional materials for applications in flexible electronic devices, including pressure/strain sensors, triboelectric nanogenerators, and actuators.

Jingxian Jiang received her B.E. degree in Chemical Engineering and Technology from Zhejiang University in 2014. She is a PhD student of Chemical Engineering and Technology at Zhejiang University and a visiting PhD student at the University of Wisconsin–Madison under the supervision of Prof. Shaoqin Gong. Her current research focuses on biomass aerogel preparation for applications in water remediation and energy storage and conversion.

Professor Feng Xu received a PhD degree from the South China University of Technology in 2005. She was a visiting scholar at the Forest Products Laboratory, United States Department of Agriculture (USDA), from 2008 to 2009. She was awarded the National Science Fund for Distinguished Young Scholars in 2012. She is currently a Chang–Jiang Scholar Distinguished Professor at the College of Materials Science and Technology, Beijing Forestry University. Her current research is focused on the isolation and identification of chemical components in wood, the development of biomass-derived functional materials, and green cellulose solvent.

Professor Shaoqin Sarah Gong received dual Bachelor's degrees in Materials Science and Engineering and Economics and Management from Tsinghua University. She also earned a Master's degree from Tsinghua University in Materials Science and Engineering, and a PhD degree from the University of Michigan–Ann Arbor in Materials Science and Engineering. She is currently a Vilas Distinguished Achievement Professor in the Department of Biomedical Engineering and the Wisconsin Institute for Discovery at the University of Wisconsin–Madison. Her current research focuses on the development of multifunctional nanomaterials and flexible devices.